Characteristics of NiO present in solids obtained from hydrotalcites based on Ni/Al and Ni-Zn/Al

Edgardo Meza-Fuentes [a], Johana Rodriguez-Ruiz [b] & Maria do Carmo Rangel [c]

[a] Grupo de Estudios en Materiales y Combustibles, Universidad de Cartagena, Cartagena, Colombia. emezaf@unicartagena.edu.co
[b] Grupo de Investigación en Procesos de la Industria Petroquímica, SENA-Centro para la Industria Petroquímica, Cartagena, Colombia. ji.rodriguez@misena.edu.co
[c] Universidade Federal do Rio Grande do Sul, Porto Alegre, Brasil. maria.rangel@ufrgs.br

Abstract
NiO has a variety of applications, mainly in the production of electrochemical sensors and of metallic nickel. In addition, it is widely used as catalysts to produce hydrogen from natural gas. In this work, hydrotalcites based on nickel-aluminum and nickel-zinc-aluminum were synthesized, calcined at 500 °C and studied by different techniques. It was observed that nickel-aluminum hydrotalcites are thermally more stable, collapsing at higher temperatures than hydrotalcites containing zinc. During calcination, aluminum is incorporated into NiO lattice, leading to a decrease in crystallographic parameters. However, zinc decreases this effect, favoring the formation of NiO with lattice parameters close to pure nickel oxide. Zinc also contributes to the formation of smaller NiO particles, which is very useful for its use as a catalyst. In addition, aluminum led to a distortion in NiO lattice, an effect that is minimized by zinc, showing that it hinders the incorporation of Al3+ in the NiO lattice.

Keywords hidrotalcite; NiO; lattice parameters; spectroscopy Raman.

Características del NiO presente en solidos obtenidos de hidrotalcitas del tipo Ni/Al y Ni-Zn/Al

Resumen
El NiO es útil en la producción de sensores electroquímicos y para la obtención de níquel metálico, el cual es usado como catalizador para producir hidrogeno a partir de gas natural. En este trabajo, se sintetizaron hidrotalcitas a base de níquel-aluminio y níquel-zinc-aluminio, las cuales fueron calcinadas a 500 ºC y estudiadas por diferentes técnicas instrumentales. Se observó que las hidrotalcitas a base de níquel y aluminio son más estables térmicamente, colapsando a temperaturas más altas que aquellas conteniendo zinc. Durante el proceso de calcinación el aluminio se incorpora en la red cristalina del NiO, disminuyendo los parámetros cristalográficos de este óxido. La adición de zinc disminuye este efecto, contribuyendo además con la formación de partículas más pequeñas del NiO. Adicionalmente el aluminio distorsiona la red del NiO, efecto que es minimizado por el zinc, dificultando la incorporación de Al^{3+} en la red cubica del NiO.

Palabras clave: hidrotalcitas; NiO; parámetros de red; espectroscopia Raman.

1. Introduction

In recent years the development of nanotechnology has contributed to important advances in areas such as catalysis, electrochemistry, design of solar cells and mobile devices, etc. In this context, nickel oxide (NiO) in the form of nano-particles or nano-films has properties that allow its use in heterogeneous catalysis, photocatalysis, manufacture of photovoltaic cells, supercapacitors and gas sensors [1-8]. In addition, nickel oxide has a band gap between 3.4 and 4.0 EV, which allows its potential use in the manufacture of capacitors for electronic instruments [9-11]. The main industrial use of NiO is related to its catalytic activity for the production of hydrogen from natural gas through the reactions of steam reforming and dry reforming with carbon dioxide [12-16]. Because NiO has a low specific surface area,

its use in heterogeneous catalysis requires a previous dispersion in supports based on activated carbon, zeolites, silica and especially alumina, which gives the final solids greater surface area, thermal and mechanical resistance, also allowing for the obtainment of small particles of NiO on the support and greater catalytic activity [1,2,14-17]. The chemical properties of metallic nickel particles obtained by reduction reactions of NiO deposited on the surface of alumina, depends on the degree of interaction of this oxide with the support, which influences the crystallinity and the size of the particles supported. In order to obtain nano-particles of nickel oxide, several investigations have been carried out in which the synthesis methods have been varied, highlighting the sol-gel and co-precipitation methods, spray pyrolysis, hydrothermal methods, etc., which aim to obtain a good dispersion of NiO on the supports [1,7,9,12-18].

In the area of materials synthesis, there is a type of compounds called layered double hydroxides (LDH) or hydrotalcites (HTLc), which, when decomposed by the effect of heat, give rise to mixtures of metal oxides with excellent properties for use in catalysis [1,17,18]. The structure of hydrotalcites and analogous materials is represented by the general formula: $[M(II)_{1-x} M(III)_x (OH)_2][A^{n-}]_{x/n} \cdot mH_2O$, where M(II)) and M(III) are metal cations located in the center of octahedral configurations and linked to six OH- groups that share their sides with other octahedral centers, thus forming infinite layers positively charged, separated from each other by anions represented by A^{n-} in the general formula and whose function is to stabilize the charge generated by the incorporation of cations with oxidation state 3+ in the crystalline lattice of the hydroxide of a divalent metal, being

the carbonate one of the anions that gives greater stability to structures of the HTLc type, due to its relative low size and high charge (2-) [17-20]. Additionally, in the free spaces between the layers, water molecules (mH_2O) are deposited, offering greater stabilization to the structure. Fig. 1 illustrates the general scheme of the hydrotalcites containing the carbonate as charge-compensating anion.

The hydrotalcites-like compounds, due to their chemical properties, can originate a wide variety of products by effect of thermal treatments, producing mixed oxides or mixtures of oxides, with properties that allow them to be used for different purposes, among which are the high specific surface area, good thermal stability, high dispersion and basic character, reasons why these materials have generated much interest and application in catalysis and in other areas [16,17,21,22].

This research work, by using thermogravimetry, studied the process of formation of NiO by the effect of heating of hydrotalcites based on Ni-Al and Ni-Zn-Al, which were previously used in the preparation of catalysts for the WGS reaction [1], which were highly selective to the production of hydrogen due to the addition of zinc. This study also seeks to expand the explanation of the effect of aluminum and zinc on the cell parameters of the NiO formed from the hydrotalcites and how this affects the crystalline lattice of the solids obtained [1].

2. Experimental

2.1. Materials synthesis

The hydrotalcites were prepared by the salt-base method and precipitation at constant pH. For the synthesis of nickel and aluminum-based solids, saline solutions based on $Ni(NO_3)_2 \cdot 6H_2O$ (98.5 %, Vetec-Sigma Aldrich, reactive grade) and $Al(NO_3)_3 \cdot 9H_2O$ (98.0%, Vetec-Sigma Aldrich, reactive grade) were previously prepared in the Ni/Al = 3 and 2 molar ratios, and alkaline solutions based on KOH (85.0 %, Merck, reactive grade) and K_2CO_3 (99.0 %, Merck, reactive grade), maintaining, between the saline and alkaline solutions, $Al/CO_3 = 2$ the molar ratio, in order to comply with the $(A^{n-})_{x/n}$ factor of the structural formula of the hydrotalcites. During this process, 200 mL of the two types of solutions were added to 400 mL of deionized water using a peristaltic pump, maintaining the system under agitation and controlling the pH at 8.2. The precipitate formed was filtered and dried at 60 ° C for 24 h. Subsequently, the materials were calcined at 500 ° C for 4 h, under air flow of 100 mL/min.

In the case of zinc-containing materials, the process carried out was similar, with the difference of adding, in the saline solutions, the compound $Zn(NO_3)_2 \cdot 6H_2O$ (98.0%, Vetec-Sigma Aldrich, reactive grade), in molar ratios Ni/Zn = 2 and 1.

Two bimetallic hydrotalcites based on nickel-aluminum; and four trimetallic hydrotalcites based on nickel-zinc-aluminum were synthesized by using the method previously described. The structural formulas and codes used for their identification are shown in Table 1.

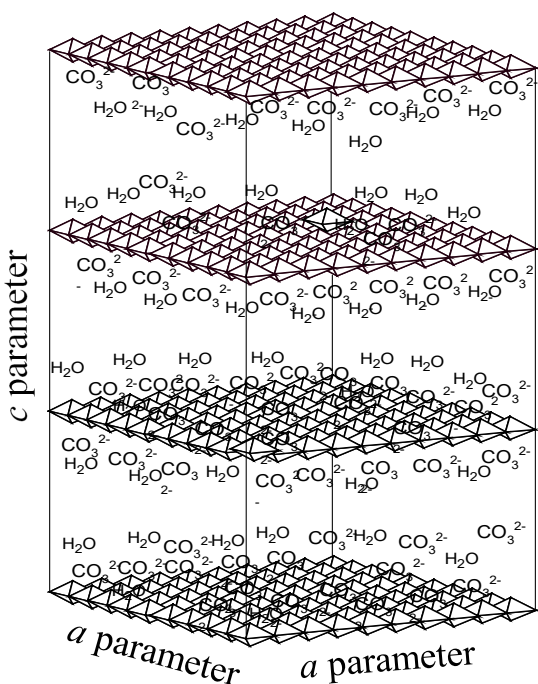Additionally, a NiO sample was synthesized from the

Figure 1. General illustration of hydrotalcite structure, in which the positive sheets formed by octahedrons, as well as carbonate anions, and interlaminar water molecules are present.
Source: The Authors.

Table 1.
Basic structural formulas of the synthesized hydrotalcites and codes used for their identification.

Structural Formula	Code
$[Ni_{0.75}Al_{0.25}(OH)_2]\,(CO_3^{2-})_{0.125}\cdot yH_2O$	$N_{0.75}A_{0.25}$
$[Ni_{0.66}Al_{0.33}(OH)_2]\,(CO_3^{2-})_{0.165}\cdot yH_2O$	$N_{0.66}A_{0.33}$
$[Ni_{0.50}Zn_{0.25}Al_{0.25}(OH)_2]\,(CO_3^{2-})_{0.125}\cdot yH_2O$	$N_{0.50}Z_{0.25}A_{0.25}$
$[Ni_{0.37}Zn_{0.37}Al_{0.25}(OH)_2]\,(CO_3^{2-})_{0.125}\cdot yH_2O$	$N_{0.37}Z_{0.37}A_{0.25}$
$[Ni_{0.44}Zn_{0.22}Al_{0.33}(OH)_2]\,(CO_3^{2-})_{0.165}\cdot yH_2O$	$N_{0.44}Z_{0.22}A_{0.33}$
$[Ni_{0.33}Zn_{0.33}Al_{0.33}(OH)_2]\,(CO_3^{2-})_{0.165}\cdot yH_2O$	$N_{0.33}Z_{0.33}A_{0.33}$

Source: The Authors.

calcination of $Ni(OH)_2$ at 500 °C, which was used as a reference for X-ray diffraction studies.

2.2. Characterization of materials

Non-calcined materials were characterized by X-ray diffraction (XRD) and thermogravimetry analysis (TGA and DTG), while calcined solids were studied using X-ray diffraction (XRD) and Raman spectroscopy techniques.

Thermogravimetry analyzes were performed in a TA Instruments equipment, model SDT 2670. In this study, 15 mg of the samples were subjected to heating from 30 to 800 °C, using a heating rate of 10 °C/min, under air flow of 50 mL/min.

X-ray diffraction studies were obtained in a Shimadzu equipment, model XDR-600, in the range 5-80 2θ, using Cu Kα radiation generated at 40 kV and 30 mA. The equipment was previously calibrated with a certified silicon standard.

In this study, through the integration of the peak corresponding to the plane (2 0 0) of the NiO, using a psdVoigt 1 type model, the values of cell parameter for the cubic lattice of this oxide were obtained, as well as the interplanar distance and particle size using the equations of Bragg (Equation 1) and Scherrer (Equation 2), respectively.

$$n\lambda = 2d\,sen(\theta) \qquad (1)$$

$$\tau = \frac{0.9\lambda}{\beta\cos(\theta)} \qquad (2)$$

Whereby λ corresponds to the wavelength used (1.5406 Å), d is the interplanar distance, θ is the value of the angle at which the diffraction peaks are centered and β is the full width at half maximum of the selected peak.

Raman spectroscopy analyzes were performed on a LabRAM HR-UV 800 / Jobin-Yvon, equipped with two He-Ne (l = 632 nm) and Ar (l = 514 nm) lasers, with a resolution of 1 mm³ and focusing the sample in an optical microscope with 10x; 50x; 100x lenses, and using a CCD detector at -70 C. For this analysis, pellets of the samples were prepared, which were subsequently positioned in the equipment by using the optical microscope and analyzed in the range of 200 to 1100 cm⁻¹.

3. Results and discussion

The X-ray diffractograms of the non-calcined solids are shown in Fig. 2. The characteristic peaks of the hydrotalcite

type structure (JCPDS 89-0460) were observed in all materials, where the ones corresponding to the planes (0 0 3), (0 0 6), (0 1 2) and (1 1 0) stand out due to their intensity.

All the materials showed the superposition of the planes (0 0 9) and (0 1 2), which appear at similar interplanar distances, which is characteristic of hydrotalcites with a high degree of purity. In diffractograms no peaks corresponding to the hydroxides or carbonates of the metals present were evident, nor of any other species, which indicates the effectiveness of the synthesis method used. The main difference was observed between the diffractograms with the same aluminum content (x = 0.25 or 0.33) whereby it was observed that, in the range of 59-63.5 ° (Figs. 2b and 2d), the shift of the peak (1 1 0) occurred at values below 2θ when the zinc content increased in the materials, which leads to the increase of the interplanar distance in the directions of the a parameter (Fig. 1) of the HTLc type structure due to the greater ionic radius of the Zn^{2+} cation with respect to Ni^{2+} and Al^{3+} [17].
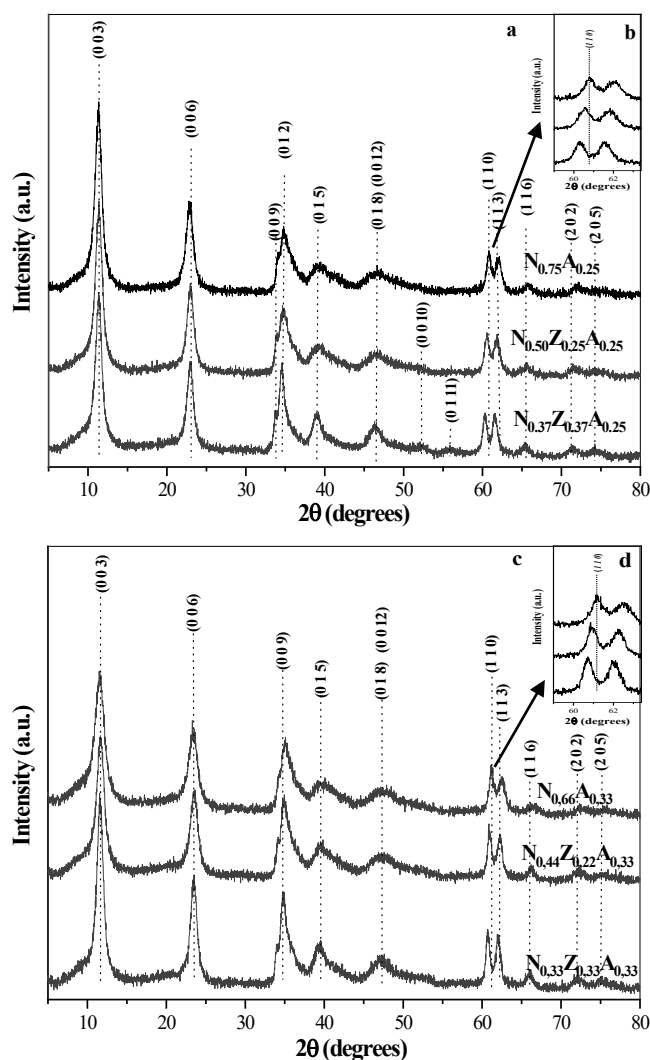

Figure 2. X-ray diffractograms of non-calcined solids: $N_{0.75}A_{0.25}$, $N_{0.50}Z_{0.25}A_{0.25}$ y $N_{0.37}Z_{0.37}A_{0.25}$ (a) y $N_{0.66}A_{0.33}$, $N_{0.44}Z_{0.22}A_{0.33}$ y $N_{0.33}Z_{0.33}A_{0.33}$ (c). Figures (b) and (d) correspond to the 59-63.5 ° range.
Source: The Authors.

The non-calcined solids gave rise to mass loss curves that indicate the phenomena that occur during the decomposition process of the hydrotalcites until the formation of the oxides from the metals which are present in the starting materials.

Fig. 3 shows that bimetallic solids ($N_{0.75}A_{0.25}$ and $N_{0.66}A_{0.33}$) presented similar thermal behaviors. Such solids registered an initial mass loss from 30 °C to approximately 250 °C, event attributable mainly to the exit of physisorbed and interlaminar water molecules, as well as to the beginning of the decomposition of the OH^- and CO_3^{2-} species present in the hydrotalcites [17].

These processes originated peaks in the DTG curve at 220 ° C and 231 ° C for the bimetallic materials, which indicates that, at these temperatures, the highest exit velocity for the material in the solids previously described can be recorded. Subsequently, an abrupt decrease in mass loss was observed in the curve, which is attributed to the collapse of the structure [17,19,23].

The initial mass loss was also reported by solids containing zinc (Fig. 3); however, the presence and increase of the content of this element leads to a decrease in the temperature needed for the collapse to occur. Similarly, it was observed that solids with higher aluminum content showed greater thermal stability when compared to those in which the Ni / Zn ratio does not vary.

After the collapse of the structure, all the solids displayed a second stage of mass loss, which is attributed to the decomposition of the hydroxide and carbonate groups, starting the formation of NiO and ZnO [23]. This process was extended to higher temperatures in solids containing higher aluminum content, which confirms that this element provides the materials with greater thermal stability, which is a fact

Table 2.
Mass percentages associated with the events recorded in the thermogravimetry curves of the hydrotalcites.

Sample	1st event (%)	2nd event (%)	3rd event (%)	Mass lost (%)
$N_{0.75}A_{0.25}$	12,97	16,51	6,70	36,18
$N_{0.66}A_{0.33}$	14,92	17,51	4,53	37,06
$N_{0.50}Z_{0.25}A_{0.25}$	12,35	17,84	4,69	34,88
$N_{0.37}Z_{0.37}A_{0.25}$	12,13	17,54	4,75	34,42
$N_{0.44}Z_{0.22}A_{0.33}$	13,67	17,23	4,10	35,00
$N_{0.33}Z_{0.33}A_{0.33}$	12,35	17,84	4,69	34,88

Source: The Authors.

that may be related to the lower contact between Ni^{2+} and/or Zn^{2+} species to form the particles of their respective oxides. The DTG curves show, in the case of bimetallic solids, peaks attributed to the formation of NiO at 329 ° C and at 359 ° C for $N_{0.75}A_{0.25}$ and $N_{0.66}A_{0.33}$, respectively [23].

For trimetallic hydrotalcites, another peak or superposition of peaks in the form of shoulders was observed at temperatures close to 280 ° C. At higher temperatures, a third event was recorded where the velocity of mass loss decreases notably, which is possibly related to the formation of transition alumina and the total decomposition of species that could become occluded in the materials by effect of the collapse. Table 2 contains the mass percentages associated with the three main events observed in TGA and DTG curves, noting that the second stage lost more mass and that the total mass released by the heating effect is quite similar for all materials.

X-ray diffractograms of calcined materials are shown in Fig. 4. In all cases, peaks of the NiO phase were observed, which, as previously evidenced by the thermogravimetry curve, is formed at the 300-360 °C range, depending on the composition of the starting solids.

Peaks that indicate the presence of ZnO were also observed, as well as the absence of peaks attributable to the presence of aluminum oxides, which can form phases with an amorphous character that does not allow for their identification by XRD.

Fig. 4 shows that the reference sample of NiO displays differences with respect to the position, width and symmetry of the peaks corresponding to the NiO present in the solids obtained by calcining the hydrotalcites, which is evidence that suggests the existence of particles of this species with smaller dimensions and dispersed in the surface of the materials obtained from hydrotalcites.

In the materials containing nickel and aluminum, the peaks of the NiO phase appear at values of 2θ higher than those shown by the reference material, which indicates a decrease in the dimensions of the nickel oxide cubic cell; this fact is verified through the values of the interplanar distance for the plane (2 0 0), shown in Fig. 5. This characteristic in bimetallic solids can be explained by admitting the insertion of Al^{3+} cations (0.69 Å) in the NiO crystal lattice, which, due to the lower ionic radius of aluminum, leads to the decrease in the dimensions of nickel oxide cubic cells [16]. The insertion of Al^{3+} into the nickel oxide structure is possible because the size of the aluminum cation does not differ by more than 15% from that of the Ni^{2+} cation (0.72 Å), and it crystallizes in the cubic system in the form of transition
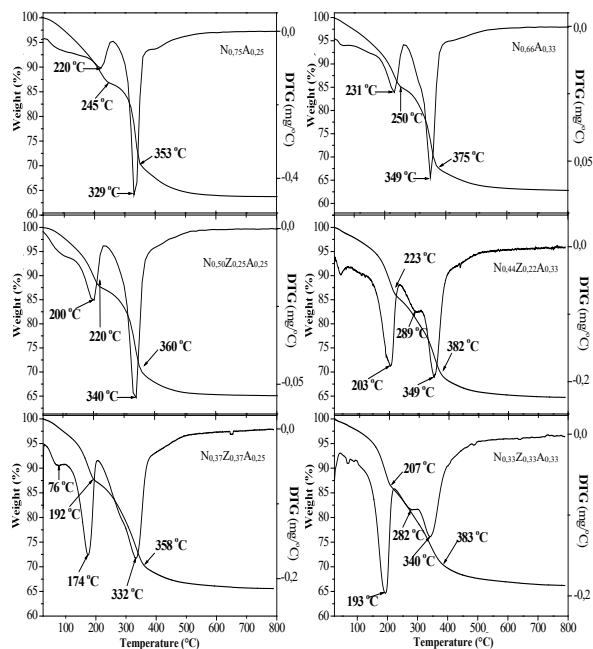

Figure 3. Mass loss and temperature differential curves from hydrotalcites to bimetallic based on nickel-aluminum and to trimetallic based on nickel-zinc-aluminum.
Source: The Authors.

alumina that can be formed by calcination and also has an electronegativity close to that of nickel, which complies with three of the Hume-Rothery rules [24], decreasing the interplanar distance in the nickel oxide due to the cationic substitution.

The higher temperature observed for the formation of NiO in nickel-aluminum-based solids may be related to the presence of aluminum-based species in the initial particles of NiO, which makes it difficult to approach the first nuclei and the formation of agglomerates of the oxide described above.

In solids containing zinc, the peaks of the NiO phase shift to values below 2θ, indicating that the presence of this element leads to an event opposite to that induced by aluminum, which suggests that zinc is also incorporated into the NiO lattice, and that having Zn^{2+} (0.74 Å), an ion radius greater than Ni^{2+} (0.72 Å) leads to an increase in the dimensions of the NiO cubic cell [1,16]. This fact is verified by the data of the interplanar distance shown in Fig. 5, in
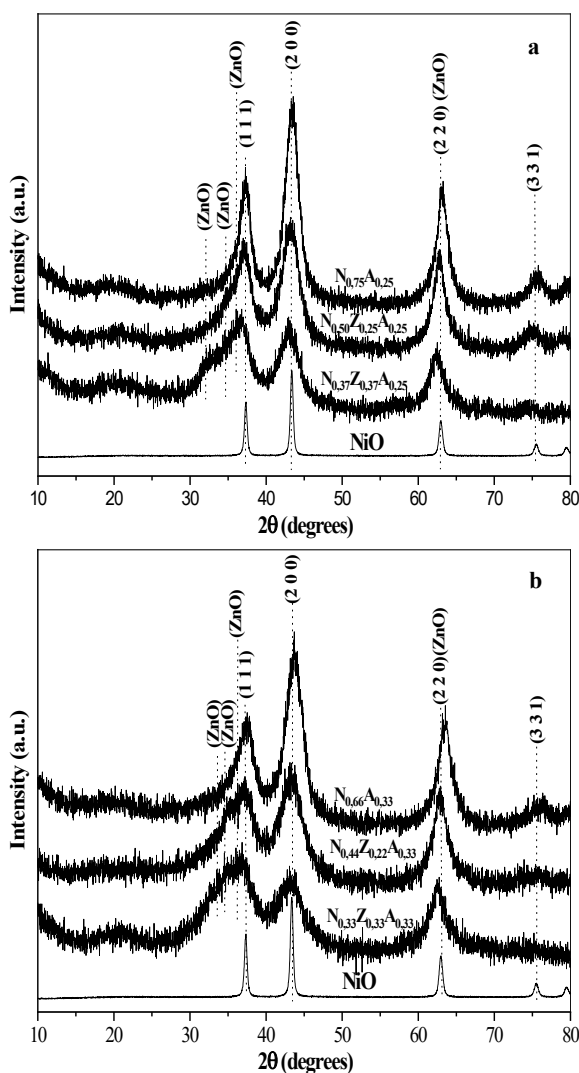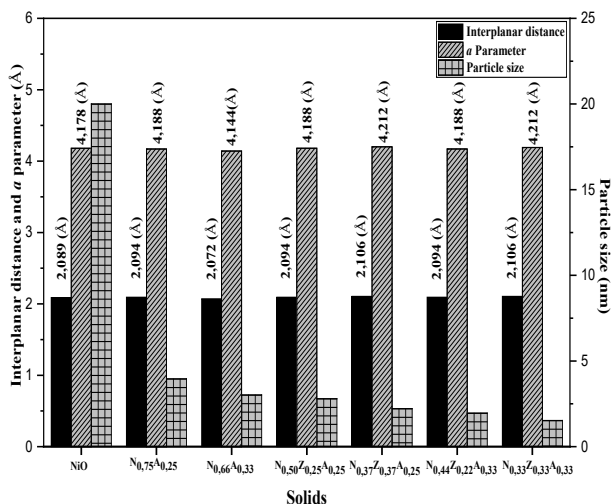

Figure 5. Interplanar distance values (d), *a* parameter, and the particle size (τ) of the NiO present in the calcined solids (τ) were calculated by applying the Scherrer equation to data obtained from the plane (2 0 0). *a* parameter was calculated through the *a = 2d* ratio, corresponding to the plane (2 0 0) of the cubic structure of the NiO.
Source: The Authors.

which it can also be observed that, when the content of nickel in the solids decreases, the particles formed are also smaller. This may be related to the presence of particles of aluminum and zinc species, which, exactly in the same way as within bimetallic solids, also discourage the formation of large NiO agglomerates. In the case of pure NiO particles, the registered size was 19.6 nm, while, in the solids obtained from hydrotalcites, the particles were less than 5 nm in all cases, as shown in Fig. 5.

The incorporation of species such as aluminum or zinc led to variations in the crystalline structure of the NiO present in the materials. This also affected the vibrational modes of NiO, which were monitored through the Raman spectra of solids. The Raman spectrum of nickel oxide has five bands originated from optical vibrations produced by one phonon (1P) of the transverse optical types (TO-440 cm^{-1}) and longitudinal optical (LO-560 cm^{-1}) and by two phonons (2P) that are the result of the coupling of the TO + TO (730 cm^{-1}), TO+LO (930 cm^{-1}) and LO + LO (1080 cm^{-1}) modes [25-28]. The Raman spectra of the $N_{0.75}A_{0.25}$ and $N_{0.66}A_{0.33}$ materials (Fig. 6), mainly displayed the bands originated by the vibrations of one phonon (1P), located at 442 and 548 cm^{-1}. Small bands at 960 and 1030 cm^{-1} were also noticed, which were associated to the LO+TO and 2LO vibrations, whereas bands related to the other modes of vibration were not identified. The bands produced by one phonon are characteristic of nickel oxide with alterations in its crystalline structure, which may be due to vacancies produced by the non-stoichiometric $Ni_{1-x}O$ oxide, or due to the presence of some Ni^{3+} cations in the structure, which was evidenced by the dark gray tonality shown by the nickel-aluminum solids [26-29]. This fact indicates the presence of crystalline defects caused by the presence of aluminum in the crystal structure of NiO, favoring the presence of type 1P vibrations, which, by not interacting with each other, discourage the coupling of

Figure 4. X-ray diffractograms of materials calcined at 500 ° C. (a; *x* = 0.25), (b; *x* = 0.33). The NiO diffractogram is used as a reference to verify peak shift due to the presence of aluminum and zinc in the structure of the NiO.
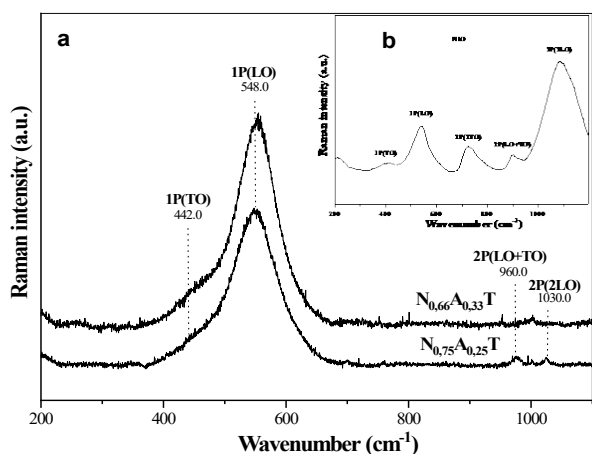Source: The Authors.

Figure 6. Raman spectra of solids $N_{0.75}A_{0.25}$ and $N_{0.66}A_{0.33}$ (a), the NiO (b) spectrum was obtained from data imported from RRUFF Project Website (rruff.info/R080121).
Source: The Authors.

the modes that cause the type 2P vibrations. It was also observed that the spectrum of the $N_{0.66}A_{0.33}$ solid shows a more pronounced shoulder of the TO vibration (442 cm^{-1}) and a sharper and more intense band, due to the LO vibration (548 cm^{-1}), which confirms that this solid contains more defects than the $N_{0.75}A_{0.25}$ sample. This was also observed by the lower value of a parameter of the nickel oxide cubic cell of the sample $N_{0.66}A_{0.33}$ (4,144 Å, see Fig. 5) caused by a greater number of Ni^{2+} cations substituted by Al^{3+}.

The Raman spectra of the materials containing nickel, aluminum and zinc are shown in Fig. 7. In all cases, signals originated from the presence of NiO and ZnO in the composition of the materials were observed. In these materials, the ZnO produced in the spectra bands attributed to optical vibrations in the range of 300-400 cm^{-1}, as a result of the superposition of the TO-E_2 (336 cm^{-1}) and TO-A_1 (381 cm^{-1}) modes, as well as bands at 413 cm^{-1} and 588 cm^{-1} due to the TO-E_1 and LO-E_1 modes, respectively [30,31].

The addition of zinc led to the presence of bands of the 2P of the NiO (TO + TO, LO + LO and TO + LO) type, caused by the coupling of vibrations in a more ordered crystalline structure of NiO, which indicates that the Zn decreases the effect of aluminum in the NiO crystal lattice, mainly in the materials in which the amount of zinc moles is half the content of Ni moles.

Fig. 8 illustrates in 2D how the vibrational modes of NiO are affected by the presence of aluminum and zinc. The incorporation of aluminum in the structure of the NiO decreased cell parameters, keeping the longitudinal and transverse modes from matching, thus making it difficult for the modes to overlap (Fig. 8a). The addition of zinc leads to a lower incorporation of aluminum in the lattice, which increases the crystallinity and the possibility of the coupling of the vibrational modes observed by Raman and illustrated in Fig. 8b. This confirms that the addition of zinc decreases the interaction, at a structural level, between the aluminum species and nickel oxide, allowing for the obtainment of particles with cell parameters close to that deployed by pure NiO.
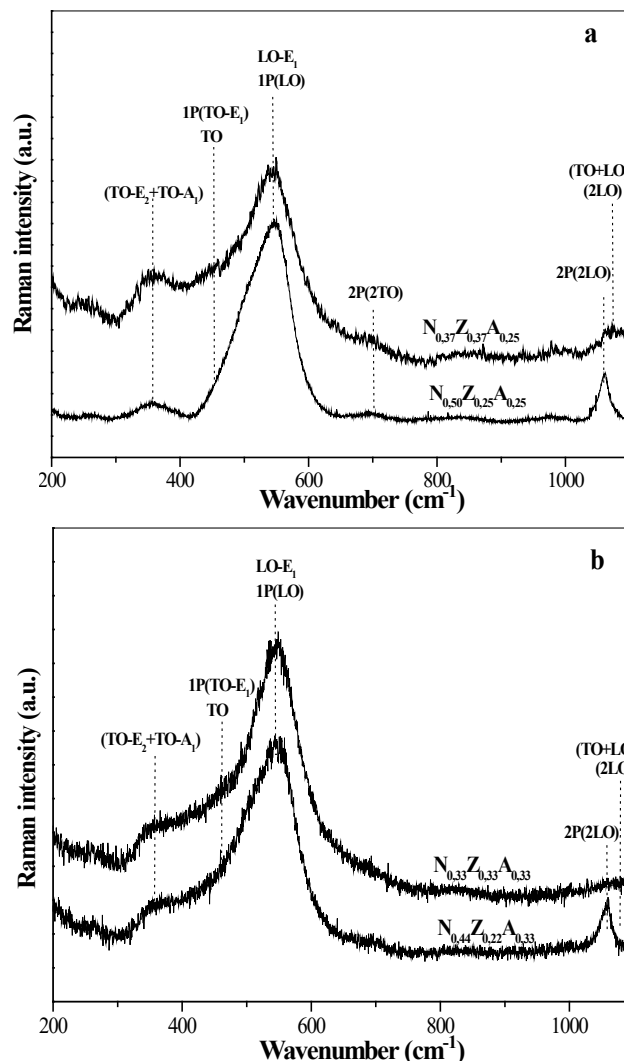

Figure 7. Raman spectra of solids $N_{0.50}Z_{0.25}A_{0.25}$ and $N_{0.37}Z_{0.37}A_{0.25}$ (a), $N_{0.44}Z_{0.22}A_{0.33}$ y $N_{0.33}Z_{0.33}A_{0.33}$ (b).
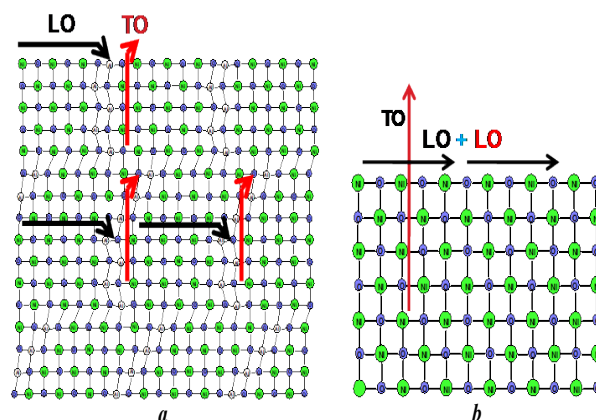Source: The Authors.

Figure 8. 2D representation of the vibrational modes present in; a) $N_{0.75}A_{0.25}$ and $N_{0.66}A_{0.33}$ solids; b) $N_{0.50}Z_{0.25}A_{0.25}$, $N_{0.37}Z_{0.37}A_{0.25}$, $N_{0.44}Z_{0.22}A_{0.33}$ and $N_{0.33}Z_{0.33}A_{0.33}$ solids.
Source: The Authors.

4. Conclusions

The increase in aluminum leads to an increase in the collapse temperature of structures of the hydrotalcite type and to a decrease in the cubic cell dimensions of the nickel oxide formed by calcining these materials at 500 °C. This effect is counteracted by the addition of zinc to the starting materials, resulting in NiO particles with larger crystalline cell sizes. The solids with the highest zinc content had the smallest particle sizes of NiO and a degree of crystallinity that allowed for the observation of bands characteristic of the coupling of the typical vibrational modes of nickel oxide with a high degree of crystallinity and that, due to the presence of the aluminum in the NiO lattice, were not clearly observed in nickel-aluminum-based materials; this indicates that zinc prevents or decreases the incorporation of Al^{3+} species in the cubic cell of NiO, thus increasing the crystallinity of nickel oxide particles.

Acknowledgments

References

[1] Meza-Fuentes, E., Cadete-Santos, F., Prakash, S., da Costa-Faro, A., de Freitas-Silva, T., Mansur-Assaf, J. and Rangel, M., The effect of metal content on nickel-based catalysts obtained from hydrotalcites for WGSR in one step. International Journal of Hydrogen Energy, 39, pp. 815-828, 2014. DOI: 10.1016/j.ijhydene.2013.10.114

[2] Meza, E., Faro, A., de Freitas, T., Assaf, J. and Rangel, M., A comparison between copper and nickel-based catalysts obtained from hydrotalcite-like precursors for WGSR. Catalysis Today, 171, pp. 290-296, 2011. DOI: 10.1016/j.cattod.2011.03.082

[3] Yuvakkumar, R., Suresh, J., Nathanael, A., Sundrarajan, M. and Hong, S., Rambutan (Nephelium lappaceum L.) peel extract assisted biomimetic synthesis of nickel oxide nanocrystals. Materials Letter, 128, pp. 170-174, 2014. DOI: 10.1016/j.matlet.2014.04.112

[4] Yu, Y., Xia, Y., Zeng, W. and Liu, R., Synthesis of multiple networked NiO nanostructures for enhanced gas sensing performance. Materials Letter, 206, pp. 80-83, 2017. DOI: 10.1016/j.matlet.2017.06.119

[5] Xia, Q., Zhao, H., Teng, Y., Du, Z., Wang, J. and Zhang, T., Synthesis of NiO/Ni nanocomposite anode material for high rate lithium-ion batteries. Materials Letter, 142, pp. 67-70, 2015. DOI: 10.1016/j.matlet.2014.11.142

[6] Kaura, N., Zappa, D., Ferroni, M., Poli, N., Campanini, M., Negrea, R. and Comini, E., Branch-like NiO/ZnO heterostructures for VOC sensing. Sensors and Actuators B: Chemical, 262, pp. 477-485, 2018. DOI: 10.1016/j.snb.2018.02.042

[7] Zhao, S., Yi, H., Tang, X., Kang, D., Gao, F., Wang, J., Huang, Y. and Yang, Z., Calcined ZnNiAl hydrotalcite-like compounds as bifunctional catalysts for carbonyl sulfide removal. Catalysis Today, Article in Press. DOI: 10.1016/j.cattod.2018.05.011

[8] Zhang, S., Pang, Y., Wang, Y., Dong, B., Lu, S., Li, M. and Ding, S., NiO nanosheets anchored on honeycomb porous carbon derived from wheat husk for symmetric supercapacitor with high performance. Journal of Alloys and Compounds, 735, pp. 1722-1729, 2018. DOI: 10.1016/j.jallcom.2017.11.294

[9] Lang, F., Sun, D., Liu, J., Wang, H. and Yan, H., Improved size-tunable synthesis of monodisperse NiO nanoparticles. Materials Letter, 181, pp. 328-330, 2016. DOI: 10.1016/j.matlet.2016.06.056

[10] Kalam, A., Al-Shihri, A., Al-Sehemi, A., Awwad, N., Du, G. and Ahmad, T., Effect of pH on solvothermal synthesis of β-Ni(OH)2 and NiO nano-architectures: surface area studies, optical properties and adsorption studies. Superlattices and Microstructures, 55, pp. 83-97,

2013. DOI: 10.1016/j.spmi.2012.11.024

[11] Tian, K., Wang, X., Li, H., Nadimicherla, R. and Guo, X., Lotus pollen derived 3-dimensional hierarchically porous NiO microspheres for NO2 gas sensing. Sensors and Actuators B: Chemical, 277, pp. 554-560, 2016. DOI: 10.1016/j.snb.2015.12.104

[12] Oliveira, E., Grande, C. and Rodrigues, A., Steam methane reforming in a Ni/Al2O3 catalyst: kinetics and diffusional limitations in extrudates. The Canadian Journal Chemical Engineering, 87, pp. 945-956, 2009 DOI: 10.1002/cjce.20223

[13] Osaki, T. and Mori, T., Role of Potassium in Carbon-free CO2 reforming of methane on K-promoted Ni/Al2O3 catalysts. Journal of Catalysis, 204, pp. 89-97, 2001. DOI: 10.1006/jcat.2001.3382

[14] Jiang, Z., Liao, X. and Zhao, Y., Comparative study of the dry reforming of methane on fluidised aerogel and xerogel Ni/Al2O3 catalysts. Applied Petrochemical Research, 3, pp. 91-99, 2012. DOI: 10.1007/s13203-013-0035-9

[15] Touahra, F., Sehailia, M., Ketir, W., Bachari, K., Chebout, R., Trari, M., Cherifi, O. and Halliche, D., Effect of the Ni/Al ratio of hydrotalcite-type catalysts on their performance in the methane dry reforming process. Applied Petrochemical Research, 6, pp. 1-13, 2016. DOI: 10.1007/s13203-015-0109-y

[16] Meza, E. y Rangel M., Síntesis de catalizadores de Ni/ZnO/Al2O3 para la reacción WGS a través del estudio de las propiedades estructurales y catalíticas de Ni/ZnO y Ni/Al2O3. Revista Colombiana de Química, 40, pp. 105-123, 2011. DOI: 10.15446/rev.colomb.quim

[17] Cavani, F., Trifiro, F. and Vaccari, A., Hydrotalcite-type ânionic clays: preparation, properties and application. Catalysis Today, 11, pp. 173-301, 1991. DOI: 10.1016/0920-5861(91)80068-K

[18] Crepaldi, E.L. and Barros, J., Hidróxidos duplos lamelares: síntese, estrutura, propriedades e aplicações. Química Nova, 21, pp. 300-311, 1998. DOI: 10.1590/S0100-40421998000300011

[19] Rodriguez-Ruiz, J., Pajaro-Payares, A., Meza-Fuentes, E., Síntesis y caracterización estructural de hidrotalcitas de Cu-Zn-Al. Revista Colombiana de Química, 45, pp. 33-38, 2016. DOI: 10.15446/rev.colomb.quim.v45n3.61381

[20] Bhojaraj, N., Harley, P. and Rajamathi M., Cannizzaro reactions over calcined hydrotalcite. Applied Clay Science, 147, pp. 86-89, 2019. DOI: 10.1016/j.clay.2019.03.028

[21] He, J., Wei, M., Li, B., Kang, Y., Evans, D. and Duan, X., Preparation of layered double hydroxides. Structure and Bonding, 119, pp. 89-119. 2006. DOI: 10.1007/430_006

[22] Borges, R., Ferreira, R., Rabelo-Neto, R., Noronha, F. and Hori, C., Hydrogen production by steam reforming of acetic acid using hydrotalcite type precursors. International Journal of Hydrogen Energy, 43, pp. 7881-7892, 2018. DOI: 10.1016/j.ijhydene.2018.03.028

[23] Meza. E., Solano. C., Pájaro, A., Rodriguez, J. and Rangel, M., Estudo do efeito da composição na temperatura do colapso da estrutura de Hidrotalcitas de Ní-Zn-Al. In: Memorias XXIV Congreso Iberoamericano de Catálisis, Medellín, Colombia, 2014.

[24] Massalski, T. and Mizutani, U., Electronic structure of Hume-Rothery phases. Progress in Materials Science, 22, pp. 151-262, 1978. DOI: 10.1016/0079-6425(78)90001-4

[25] Wang, W., Liu, Y., Xua, C., Zheng, C. and Wang, G., Synthesis of NiO nanorods by a novel simple precursor thermal decomposition approach. Chemical Physics Letters, 362, pp. 119-122, 2002. DOI: 10.1016/S0009-2614(02)00996-X

[26] Ni, X., Zhao, Q., Zhou, F., Zheng, H., Cheng, J. and Li, B., Synthesis and characterization of NiO strips from a single source. Journal of Crystal Growth, 289, pp. 299-302, 2006. DOI: 10.1016/j.jcrysgro.2005.10.017

[27] Mironova-Ulmanea, N., Kuzmina, A. and Grube, M., Raman and infrared spectromicroscopy of manganese oxides. Journal of Alloys and Compounds, 480, pp. 97-99, 2009. DOI: 10.1016/j.jallcom.2008.10.056

[28] Thamri, S., Sta, I, Jlassi, M., Hajji, M. and Ezzaouia, H., Fabrication of ZnO-NiO nanocomposite thin films and experimental study of the effect of the NiO, ZnO concentration on its physical properties. Materials Science in Semiconductor Processing, 71, pp. 310-320, 2017. DOI: 10.1016/j.mssp.2017.08.017

[29] Švegl, F., Šurca-Vuk, A., Hajzeri, M., Slemenik-Perše, L. and Orel, B., Electrochromic properties of Ni(1−x)O and composite Ni(1−x)O-

polyaniline thin films prepared by the peroxo soft chemistry route. Solar Energy Materials and Solar Cells, 99, pp. 14-25, 2012. DOI: 10.1016/j.solmat.2011.11.043

[30] Jang, M., Yoon, M., Lee, S., Kim, H., Onodera. A. and Kojima, S., A study on the Raman spectra of Al-doped and Ga-doped ZnO ceramics. Current Applied Physics, 9, pp. 651-657, 2009. DOI: 10.1016/j.cap.2008.05.019

[31] Tangcharoen, T., Klysubun, W. and Kongmark, C., Synthesis of nanocrystalline NiO/ZnO heterostructured composite powders by sol-gel auto combustion method and their characterizations. Journal of Molecular Structure, 1156, pp. 524-533, 2018. DOI: 10.1016/j.molstruc.2017.12.019

E. Meza-Fuentes, received the BSc. in Chemistry in 2001 from Universidad de Cartagena, Colombia, MSc. and PhD in Chemistry from Universidade Federal de Bahia, Brazil in 2006 and 2009, respectively. Currently, works as assistant professor at the Universidad de Cartagena and as director of the Group on Materials and Fuels Studies. His research interests include: heterogeneous catalysis, carbochemistry, chemometrics and environmental chemistry.
ORCID: 0000-0003-3725-8112

J. Rodríguez-Ruiz, received the BSc. in Chemistry in 2001 from Universidad de Cartagena, Colombia, and MSc. in Chemistry from Universidade Federal de Bahia, Brazil, in 2007. Currently, works as instructor at the Centro para la Industria Petroquímica-SENA, Colombia and as director of Group of Investigation in Processes of the Petrochemical Industry. His research interests include: oil analysis, synthesis and degradation of polymers, heterogeneous catalysis and environmental chemistry.
ORCID: 0000-0002-4263-4242

M.C. Rangel, received the BSc. Eng in Chemical Engineering in 1979, MSc. in Chemistry in 1985, all of them from Universidad Federal de Bahía and PhD in Chemistry in 1991 from Universidade Estadual de Campinas, Brazil. He has done postdoctoral studies at Universidad Autónoma de Madrid, Spain and at the Centre National de la Recherche Scientifique. Additionally, he has worked as coordinator of graduate programs in chemistry at Universidade Federal de Bahia and acts as a guest editor in Catalysis Today. In the 1979-2016 period, he worked as a professor and researcher at Universidade Federal de Bahia. He is currently a full-time professor at Universidade Federal de Rio Grande do Sul, Brazil. His research interests include catalytic transformations of biomass, generation and purification of hydrogen; improving the quality of diesel and gasoline; production of clean fuels; generation of synthesis gas; fuel cells and advanced oxidative processes.
ORCID: 0000-0002-2497-9837